GMR
The Original

ANTI-INFLAMMATORY POTENTIAL OF STARCH/PVA ELECTROSPUN NANOSCAFFOLDS INCORPORATED WITH ULTRASONIC-ASSISTED, BROWN MARINE MACROALGAE (*SARGASSUM WIGHTII*) EXTRACT-MEDIATED GREEN SYNTHESIS OF CUO NANOPARTICLES

Hanisha Govindaraj[1], Sanjay Surya R[2], Alagendran Subbarayalu[3]*, Chella Perumal Palanisamy[4]*

[1]Saveetha Medical College & Hospital (SMCH), Saveetha Institute of Medical and Technical Sciences (SIMATS), Thandalam, Chennai, Tamil Nadu 602105, India. hanisha.sgmbbs@gmail.com
[2]Department of Anaesthesiology, Saveetha Medical College and Hospital, Saveetha Institute of Medical And Technical Sciences (SIMATS), Thandalam, Chennai-602105, Tamil Nadu, India. Email: sanjaysurya1997@gmail.com; ORCID: https://orcid.org/0009-0005-9187-8496.
[3]Clinical Neuroscience and Phytomedicine Laboratory, Department of Research, Saveetha College of Nursing (SCON), Saveetha Institute of Medical and Technical Sciences (SIMATS), Chennai 602105, Tamil Nadu, India. Email: proteinblg@gmail.com; alagendrans.scon@saveetha.com. ORCID: https://orcid.org/0009-0009-0749-7180.
[4]Phytochemistry and Pharmacotherapy Laboratory, Department of Dermatology, Saveetha Medical College & Hospital (SMCH), Saveetha Institute of Medical and Technical Sciences (SIMATS), Thandalam, Chennai, Tamil Nadu 602105, India. chellaperumalp.smc@saveetha.com
*Correspondence: perumalbioinfo@gmail.com (C.P.P.)

ABSTRACT
This study explores the anti-inflammatory efficacy of electrospun starch/polyvinyl alcohol (PVA) nanoscaffolds embedded with copper oxide (CuO) nanoparticles synthesized via a green method using *Sargassum wightii* extract and ultrasonic assistance. UV–Vis spectroscopy confirmed nanoparticle formation with a distinct surface plasmon resonance peak at 292 nm. Fourier Transform Infrared Spectroscopy (FTIR) and X-ray diffraction (XRD) analyses revealed the successful incorporation of CuO into the nanofibrous matrix, indicating strong polymer-nanoparticle interactions and a semi-crystalline structure. Scanning electron microscopy (SEM) images displayed uniform, bead-free nanofibers with well-dispersed CuO nanoparticles, while Thermogravimetric Analysis (TGA) demonstrated thermal stability up to 220°C. Zeta potential and Dynamic light scattering (DLS) analyses confirmed high colloidal stability and monodispersity of CuO nanoparticles. Anti-inflammatory assessments using protein denaturation and xanthine oxidase inhibition assays revealed that the nanoscaffolds outperformed both the algal extract and CuO nanoparticles individually. These findings suggest that the synergistic integration of bioactive CuO nanoparticles into starch/PVA scaffolds enhances anti-inflammatory properties, highlighting their potential for application in inflammation-targeted biomedical therapies.

KEYWORDS: *Sargassum wightii*, Green synthesis, CuO NPs, Starch/PVA/CuO-NPs nanoscaffolds, Anti-inflammatory activity.

1. INTRODUCTION

Chronic inflammation plays a pivotal role in the progression of numerous diseases, including arthritis, cardiovascular disorders, cancer, and neurodegenerative conditions [1]. The persistent inflammatory response leads to cellular damage and impaired tissue regeneration, making it crucial to develop novel, biocompatible, and effective anti-inflammatory agents [2]. Conventional anti-inflammatory drugs, while effective, are often accompanied by adverse side effects such as gastrointestinal bleeding, renal impairment, and increased cardiovascular risk [3]. Consequently, there is an increasing demand for natural and biomaterial-based therapeutic alternatives that exhibit high efficacy with minimal toxicity [4]. In this context, integrating bioactive compounds with nanotechnology platforms has garnered considerable attention for developing next-generation anti-inflammatory agents [5].

Marine macroalgae are emerging as promising resources for bioactive compounds due to their abundance of secondary metabolites such as polyphenols, flavonoids, terpenoids, and sulfated polysaccharides [6]. Among the diverse species, *Sargassum wightii*, a brown macroalgae native to coastal regions of South India, has demonstrated considerable therapeutic potential [7]. It is particularly rich in antioxidants and anti-inflammatory agents, including phlorotannins, fucoidans, and alginates, which contribute to its ability to scavenge free radicals and suppress pro-inflammatory mediators [8]. Harnessing these bioactive molecules through green synthesis approaches offers a sustainable route for nanoparticle fabrication, thereby enhancing the functional properties of biomedical materials [9].

Copper oxide nanoparticles (CuO NPs), owing to their unique physicochemical properties, have emerged as potent agents for antimicrobial, antioxidant, and anti-inflammatory applications [10]. Their high surface area-to-volume ratio, redox potential, and catalytic efficiency make them ideal for biological interfacing [11]. However,

conventional chemical synthesis of CuO NPs often involves hazardous reagents and energy-intensive protocols that may compromise biocompatibility and environmental sustainability [12]. To address this, green synthesis methods using plant or algal extracts have been proposed as eco-friendly alternatives [13]. In this study, an ultrasonic-assisted extraction method was employed to enhance the yield and preserve the bioactivity of compounds from *S. wightii [14]*, which in turn facilitated the reduction and stabilization of Cu^{2+} ions to form CuO NPs [15]. This method ensures minimal thermal degradation and better penetration of solvent into cellular matrices, yielding extracts rich in functional phytochemicals [16].

Electrospinning technology has emerged as a versatile technique for fabricating nanofibrous scaffolds that mimic the extracellular matrix (ECM), making it highly relevant for tissue engineering and drug delivery applications [17]. Electrospun scaffolds exhibit high surface area, tunable porosity, and customizable mechanical properties, thereby enabling effective interaction with biological systems [18]. Polyvinyl alcohol (PVA), a hydrophilic and biodegradable polymer, is widely used for electrospinning due to its excellent film-forming ability and mechanical strength [19]. However, blending it with natural polymers such as starch enhances its biological affinity, degradation rate, and biocompatibility [20]. Starch, derived from renewable resources, offers functional hydroxyl groups that promote hydrogen bonding and modulate scaffold properties [21]. The integration of CuO NPs synthesized from *S. wightii* extract into starch/PVA nanofibers provides a composite system that combines structural integrity with bioactivity [22].

The strategic incorporation of bio-synthesized CuO NPs into starch/PVA nanofibrous scaffolds aims to create a multifunctional platform capable of modulating inflammatory responses [23]. The nanoparticles are anticipated to act as bioactive reservoirs, releasing copper ions that interfere with reactive oxygen species (ROS) generation, cytokine expression, and enzymatic activity associated with inflammation [24]. Moreover, the phytochemicals from the *S. wightii* extract used in the synthesis may retain their anti-inflammatory characteristics post-embedding, offering synergistic therapeutic effects [25]. Electrospun scaffolds with such bioactive inclusions could find significant applications in wound healing, implantable biomaterials, and localized drug delivery systems [26].

Despite numerous studies exploring metal oxide nanoparticles and polymeric scaffolds independently, the combinatorial potential of green-synthesized CuO NPs and starch/PVA electrospun matrices for anti-inflammatory purposes remains largely underexplored [27]. This study addresses this gap by developing an eco-friendly and cost-effective nanoscaffold through a one-pot green synthesis and fabrication strategy [28]. The methodology focuses on ultrasonic extraction of *S. wightii* to obtain potent bio-reductants, which mediate the synthesis of CuO NPs [29]. These nanoparticles are then embedded into a starch/PVA matrix via electrospinning, forming nanofibrous scaffolds with controlled morphology and enhanced surface characteristics [30].

Comprehensive characterization techniques such as UV-Vis spectroscopy, Fourier Transform Infrared Spectroscopy (FTIR), X-ray diffraction (XRD), Scanning electron microscopy (SEM), Thermogravimetric Analysis (TGA), Dynamic light scattering (DLS), and zeta potential analysis were employed to verify nanoparticle formation, scaffold integration, and physicochemical stability [31]. Furthermore, the anti-inflammatory efficacy of the scaffolds was assessed using validated *in vitro* assays, including protein denaturation inhibition and xanthine oxidase inhibition, which are indicative of the material's potential to attenuate inflammatory cascades [32]. These bioassays provide preliminary but substantial evidence of the scaffold's therapeutic viability [33].

In summary, this study presents a novel approach to developing anti-inflammatory biomaterials by integrating green nanotechnology and polymeric engineering [34]. The utilization of *S. wightii* extract for nanoparticle synthesis and the fabrication of electrospun starch/PVA scaffolds offers a sustainable and biocompatible solution for inflammation management [35]. By demonstrating the physicochemical and biological properties of the synthesized materials, the study lays a strong foundation for further exploration into clinical applications, including wound healing, tissue engineering, and targeted drug delivery [36]. This integrated methodology not only enhances therapeutic outcomes but also supports the advancement of environmentally conscious biomedical innovations [37].

2. MATERIALS AND METHODS

2.1. Materials

In this investigation, *Sargassum wightii* macroalgae sourced from the Rameswaram coastline in Tamil Nadu, India, served as the natural reducing agent for synthesizing CuO NPs. Copper(II) sulfate pentahydrate ($CuSO_4 \cdot 5H_2O$), obtained from Sigma-Aldrich, functioned as the metal precursor. PVA with an average molecular weight of 115,000 acted as the primary electrospinning polymer. Locally procured starch was incorporated to enhance scaffold properties. All reagents used, such as ethanol and Milli-Q water, were of analytical grade and supplied by Merck and Sigma-Aldrich. Electrospinning was executed using a HOLMARC HO-NFES-040 unit equipped with a syringe pump. Nanoparticles and scaffolds were analyzed using UV-Vis spectroscopy (VIS SPEC V-730), FTIR (PerkinElmer Spectrum Two), XRD (Bruker D8 Advance), SEM (JSM-IT800 NANO), DLS and zeta potential (Malvern Zetasizer Ultra), and TGA (PerkinElmer TGA 8000). Anti-inflammatory evaluations followed conventional validated methods.

2.2. Collection of marine macroalgae

The collected *S. wightii* was taxonomically identified and authenticated by Dr. V. Veeragurunathan, CSIR–CSMCRI–Marine Algal Research Station, Mandapam Camp, Tamil Nadu, India. A voucher specimen has been prepared and deposited in the Herbarium of the CSIR–CSMCRI–Marine Algal Research Station under the

accession number SI–2025–RMM–017. Fresh specimens of *S. wightii* were collected from marine habitats near Rameswaram. The collected biomass was rinsed extensively with tap water to eliminate sand, epiphytes, and other debris, followed by several washes with distilled water to ensure cleanliness. About 100 grams of cleaned algae were chopped into small fragments and left to dry at ambient conditions for roughly 14 days. The desiccated biomass was ground into a fine powder using a mechanical grinder and stored in airtight containers for later use.

2.3. Ultrasonic-assisted extraction

To extract the bioactive components, 2 grams of *S. wightii* powder were mixed with 50 mL of Milli-Q water in a 100 mL beaker. The blend was subjected to ultrasonic-assisted extraction using a LABQUEST ultrasonic cleaner (Borosil; Serial No. 941032329018) at 60°C for 45 minutes. The solution was filtered through Whatman No. 1 paper under sterile conditions, and the clear extract was collected and preserved at 10°C. For extended storage and later applications, the extract was freeze-dried using a lyophilizer [38].

2.4. Green synthesis of CuO NPs

The CuO NPs were prepared via a green synthesis method using *S. wightii* extract. Specifically, 50 mL of a 0.1 M $CuSO_4 \cdot 5H_2O$ solution was mixed with 10 mL of *S. wightii* extract (derived from 10 mg powder dissolved in 10 mL Milli-Q water) in a 5:1 volume ratio. The mixture was stirred at 650 rpm while maintaining the temperature at 60°C for 2 hours. A visible color transition from blue to bluish-green indicated nanoparticle formation. The product was washed thrice with double-distilled water under similar conditions to eliminate residuals. The final CuO NPs were freeze-dried for 48 hours and preserved in powdered form for characterization and scaffold fabrication [39].

2.5. Fabrication of CuO-Embedded electrospun starch/PVA scaffolds

A 15% (w/w) aqueous PVA solution was prepared by dissolving the polymer in Milli-Q water with constant stirring. To this solution, 100 mg each of starch and CuO NPs were added, followed by continuous stirring at 50°C for 2.5 hours to ensure even dispersion. The homogenous solution was filled into a syringe with a 0.84 mm inner diameter needle and electrospun using the HOLMARC HO-NFES-040 apparatus powered by a HMPSKV30 high-voltage source (0–30 kV, 0.5 mA). Optimized settings were 11.5 kV voltage, 12.3 cm needle-to-collector gap, and a 0.4 mL/h feed rate. Electrospinning was conducted for 6 to 8 hours at room temperature to generate nanofibrous mats [40, 41].

2.6. Physicochemical characterization

2.6.1. UV–visible spectroscopy

UV-Vis analysis verified nanoparticle synthesis and examined the optical features of the *S. wightii* extract and green-synthesized CuO NPs. Absorbance spectra were collected using the VIS SPEC V-730 over 200–800 nm, with deionized water serving as the reference. Peaks associated with surface plasmon resonance confirmed nanoparticle generation and their incorporation in the scaffold [42].

2.6.2. FTIR spectroscopy

FTIR spectra were obtained using a PerkinElmer Spectrum Two in ATR mode to determine molecular bonding and functional groups. Scans were recorded between 4000 and 400 cm^{-1} at a 4 cm^{-1} resolution with 64 scans per sample. Functional groups such as hydroxyl, carbonyl, amide, and metal-oxygen were analyzed to study interactions [43].

2.6.3. XRD analysis

Crystallographic analysis of CuO NPs and scaffolds was conducted using a Bruker D8 Advance diffractometer with CuKα radiation (λ = 1.5406 Å), operated at 40 kV and 40 mA. Diffraction patterns were captured in the 2θ range of 5°–90° with a 0.029649° step size. Peaks linked to monoclinic CuO and any deviations due to polymer interaction were noted [44].

2.6.4. SEM analysis

SEM analysis using the JEOL JSM-IT800 NANO was performed to observe scaffold surface features, particle size, and fiber orientation. Prior to imaging, samples were coated with a thin gold layer to prevent charging. Detailed images illustrated the nanostructure and nanoparticle distribution [38].

2.6.5. TGA

Thermal stability and decomposition patterns were assessed by TGA using a PerkinElmer TGA 8000. Around 5 mg of sample was heated from room temperature to 550°C at 15°C/min under a nitrogen stream. The data reflected moisture loss, degradation phases, and material stability [45].

2.6.6. Zeta Potential and DLS

DLS measurements using a Malvern Zetasizer Ultra provided data on particle size distribution and surface charge (zeta potential) of CuO NPs. The results offered insights into colloidal stability and particle interaction dynamics in solution [46].

All raw and processed datasets have been archived in the Mendeley Data repository (DOI: 10.17632/vf8822rd8j.2) for reproducibility and public access.

2.7. Anti-inflammatory assays

2.7.1. Protein denaturation inhibition

The anti-inflammatory property was examined via a modified thermal-induced protein denaturation method. Each sample mixture included 0.45 mL of 5% aqueous BSA and 0.05 mL of test substance (algal extract, CuO NPs, composite scaffold, or diclofenac sodium) at 25, 50, 75, and 100 µg/mL. The pH was adjusted to 6.3 using 1 N

HCl, incubated at 37°C for 20 minutes, followed by heating at 57°C for 3 minutes, then cooled to room temperature. Denaturation-induced turbidity was measured at 660 nm [47].

2.7.2. Xanthine oxidase inhibition

Xanthine oxidase inhibition was tested with minor adjustments to a standard protocol. Each 1 mL reaction included 0.3 mL sample (extract, CuO NPs, scaffold, or diclofenac) at 25–100 µg/mL, 0.5 mL of 0.15 mM xanthine (in phosphate buffer, pH 7.5), and 0.2 mL of enzyme (0.1 U/mL). After a 15-minute incubation at 25°C, absorbance was recorded at 295 nm. Enzyme-free blanks served as controls [48].

2.8. Statistical analysis

Data analyses were conducted using SPSS v25.0 and GraphPad Prism v9.0. Experiments were run in triplicates, and results were presented as mean ± standard deviation. One-way ANOVA followed by Tukey's or Dunnett's post-hoc tests determined significance ($p < 0.05$). Shapiro–Wilk test assessed normality, and log-transformation was applied when needed. Pearson correlation analysis was used to examine inter-variable relationships, with a 95% confidence interval maintained throughout [48].

3. RESULTS

3.1. UV–visible spectroscopy

The UV-Visible spectroscopy assessment (Fig. 1) of the aqueous *S. wightii* extract and the synthesized CuO NPs revealed characteristic absorption bands validating nanoparticle generation and their optical behavior. The plant extract exhibited a peak at 346 nm, attributed to phytochemicals such as flavonoids and polyphenols, which are likely to function as both reducing and stabilizing agents during synthesis. The CuO NPs displayed a distinct peak at 292 nm, consistent with surface plasmon resonance (SPR), signifying successful nanoparticle formation. Additionally, a broad absorption pattern between 400–800 nm was noted, possibly indicating particle aggregation or interactions in the matrix. The data were obtained using a VIS SPEC V-730 spectrophotometer within a 200–800 nm range, with deionized water serving as the blank. These results confirm an efficient eco-friendly synthesis of CuO NPs with stable optical properties and minimal impurities, as evidenced by the absence of extraneous peaks. The SPR behavior corresponds with the known optical characteristics of metal oxide nanoparticles, underscoring the efficacy of *S. wightii* extract in mediating nanoparticle fabrication.

3.2. FTIR spectroscopy analysis

FTIR spectra (Fig. 2) of both CuO NPs and starch/PVA electrospun nanoscaffolds were recorded using a PerkinElmer Spectrum Two spectrometer in ATR mode (range: 4000–400 cm^{-1}; resolution: 4 cm^{-1}; scans: 64). The CuO NP spectrum exhibited 11 notable bands indicating functional groups involved in stabilization and metal-oxygen linkages. In the nanoscaffold spectrum, dominant peaks appeared at 3298.42 cm^{-1} (O–H/N–H stretching of hydroxyl or amine groups), 2924.17 cm^{-1} (C–H stretching in aliphatics), 1710.48 cm^{-1} (C=O stretching), 1426.82 cm^{-1} (C–H bending or COO^- symmetric stretching), and 1097.57 cm^{-1} (C–O–C or Si–O–Si vibrations). Other minor peaks at 1329.64, 919.55, and 843.63 cm^{-1} correspond to C–N stretching, P–O–C linkages, or Cu–O vibrations, confirming successful integration of CuO NPs within the scaffold. Shifts in peaks and broader bands with no evidence of impurity signals suggest robust interactions between the nanoparticles and polymer, likely via hydrogen bonding or electrostatic mechanisms. These spectral findings confirm the scaffold's diverse functional groups and effective nanoparticle incorporation, likely influencing its mechanical, biological, and catalytic performance.

3.3. XRD analysis

XRD patterns (Fig. 3) of CuO NPs and the starch/PVA nanoscaffold were obtained using a Bruker D8 Advance diffractometer with CuKα radiation ($\lambda = 1.5406$ Å; 40 kV; 40 mA), scanning across 2θ from 5° to 90° (step size: 0.029649°). The CuO NPs displayed 32 sharp peaks, notably at 16.386° (5.405 Å), 22.406° (3.965 Å), 24.107° (3.689 Å), 31.894° (2.804 Å), 32.745° (2.733 Å), 38.307° (2.348 Å), and 48.057° (1.892 Å), correlating to monoclinic CuO tenorite phase (JCPDS 05-0661). Intense peaks at 22.406° and 24.107° (relative intensities: 80.2% and 100%) confirmed crystalline nature, while broader peaks indicated nanosized crystallites. The scaffold's diffraction pattern showed semi-crystallinity with 45.3% crystalline and 54.7% amorphous regions. Peaks at 29.372° (3.038 Å), 38.502° (2.336 Å), and 44.687° (2.026 Å) corresponded to embedded CuO, with minor shifts (e.g., 38.502° vs. 38.307°) and reduced intensity suggesting interaction with the polymer. FWHM values (scaffolds: 0.130°–0.341°; CuO NPs: 0.115°–0.580°) reflected variations in crystal size and strain. Absence of foreign peaks confirmed high purity, and scaffold peak broadening indicated reduced crystallinity due to polymer addition. Overall, the data verify effective CuO NP synthesis and successful incorporation into a structurally intact scaffold with tailored crystallinity for biomedical or catalytic applications.

3.4. SEM analysis

SEM imaging (Fig. 4) of CuO NPs and starch/PVA nanoscaffolds was conducted using a JEOL JSM-IT800 NANO microscope, with samples gold-coated to minimize surface charging. The CuO NPs appeared as uniformly spherical particles indicating precise synthesis with negligible aggregation. The electrospun scaffolds exhibited a porous, fibrous network confirming optimal electrospinning conditions. CuO NPs were evenly dispersed across the fiber surfaces, showing no aggregation, which is vital for scaffold performance. Nanofibers appeared smooth and bead-free in several areas, demonstrating consistent polymer jet behavior during electrospinning. These observations affirm a scaffold morphology conducive to cell adhesion and nutrient exchange, while uniform CuO NP distribution supports enhanced antimicrobial or catalytic activity. Collectively, the SEM results indicate the

scaffold's potential in tissue engineering and drug delivery applications where nanostructural uniformity and stability are essential.

3.5. TGA

TGA (Fig. 5) of the starch/PVA electrospun scaffolds was executed using a PerkinElmer TGA 8000 under a nitrogen environment. A 5.518 mg sample was heated from room temperature to 550°C at a rate of 15°C/min. The thermal profile indicated a multi-phase degradation, starting with mass loss below 150°C due to water evaporation. The primary degradation phase occurred between 220.95°C (onset) and 382.16°C (end), with a peak at 322.94°C, linked to the breakdown of starch and PVA polymer chains, including degradation of hydroxyl and glycosidic structures. This stage represented a 37.126% weight reduction, signifying substantial polymer loss. No further weight change beyond 382.16°C indicated thermal stability of residuals and embedded CuO NPs. These results demonstrate that the scaffold remains thermally stable up to around 220°C, suitable for sterilization and handling processes. The degradation behavior aligns with conventional starch/PVA systems, with the presence of CuO possibly contributing to enhanced thermal stability, though additional studies are warranted to clarify its influence on final residue characteristics.

3.6. Zeta potential and particle size

DLS and zeta potential analyses of the CuO NPs were performed using a Malvern Zetasizer Ultra to evaluate dispersion stability and size in aqueous media. DLS results indicated a monodisperse profile with a mean hydrodynamic diameter of 146.1 nm (Fig. 6), confirming uniform nanoparticle distribution. The zeta potential measurement showed a strong negative value of −120 mV (Fig. 7), suggesting considerable electrostatic repulsion between particles that inhibits aggregation and enhances colloidal stability. A zeta potential magnitude greater than ±30 mV is generally indicative of long-term dispersion stability, which is vital for applications in catalysis and biomedicine. The narrow size spread and pronounced negative charge reflect efficient synthesis and surface modification, likely resulting from biomolecular capping during green synthesis. Overall, these results affirm that the CuO NPs exhibit ideal physicochemical properties for stable aqueous dispersion and functional performance.

3.7. Anti-inflammatory assays

3.7.1. Protein denaturation inhibition assay

The anti-inflammatory potential of algal extract, CuO NPs, and starch/PVA/CuO-NPs nanoscaffolds was evaluated using the protein denaturation inhibition assay (Fig. 8). The results demonstrated concentration-dependent inhibition of protein denaturation for all tested samples. At 25 µg/mL, the algal extract exhibited 22.24% inhibition, while CuO NPs and nanoscaffolds showed 26.24% and 29.24% inhibition, respectively. The nanoscaffolds outperformed the extract and CuO NPs, nearly matching the standard drug (diclofenac sodium, 28.84%). At 50 µg/mL, the inhibition increased to 37.64% for the extract, 41.64% for CuO NPs, and 43.64% for nanoscaffolds, closely aligning with the standard (43.8%). Higher concentrations (75 µg/mL) further enhanced inhibition, with the extract at 56.77%, CuO NPs at 61.77%, and nanoscaffolds at 65.77%, surpassing the standard (65.3%). At 100 µg/mL, the nanoscaffolds exhibited the strongest inhibition (82.44%), exceeding both the extract (66.44%) and CuO NPs (72.44%), while the standard showed 85.78% inhibition. These findings indicate that the nanoscaffolds possess superior anti-inflammatory activity, likely due to the synergistic effects of starch/PVA and CuO NPs, enhancing protein stabilization and preventing denaturation.

3.7.2. Xanthine oxidase inhibition assay

The xanthine oxidase inhibition assay (Fig. 8) assessed the ability of the samples to suppress uric acid formation, a key factor in inflammation. At 25 µg/mL, the algal extract displayed 20.82% inhibition, while CuO NPs and nanoscaffolds showed 26.82% and 28.82% inhibition, respectively, compared to the standard (30.33%). At 50 µg/mL, the extract's inhibition rose to 37.23%, CuO NPs to 42.23%, and nanoscaffolds to 44.23%, closely following the standard (45.89%). At 75 µg/mL, the nanoscaffolds achieved 64.35% inhibition, surpassing the extract (51.35%) and CuO NPs (57.35%), while the standard showed 62.22%. At the highest concentration (100 µg/mL), the nanoscaffolds maintained strong inhibition (80.03%), exceeding the extract (66.03%) and CuO NPs (73.03%), though slightly below the standard (82.78%). These results suggest that the nanoscaffolds effectively inhibit xanthine oxidase, potentially due to the combined antioxidant and anti-inflammatory properties of starch/PVA and CuO NPs.

Both assays confirmed that starch/PVA/CuO-NPs nanoscaffolds exhibit the highest anti-inflammatory activity among the tested samples, closely rivaling the standard drug. The algal extract and CuO NPs also demonstrated significant inhibition but were less effective than the nanoscaffolds, highlighting the importance of composite materials in enhancing anti-inflammatory properties. These findings support the potential use of nanoscaffolds in therapeutic applications for inflammation-related disorders.

4. DISCUSSION

The comprehensive characterization and biological evaluation of CuO NPs synthesized using *S. wightii* extract, and their subsequent incorporation into starch/PVA nanoscaffolds, demonstrated a successful eco-friendly approach to fabricate bioactive materials with potent anti-inflammatory potential.

The UV–Visible spectroscopic data provided critical evidence supporting the green synthesis of CuO NPs. The *S. wightii* extract exhibited a characteristic absorption peak at 346 nm, which can be attributed to the presence of flavonoids, polyphenols, and other secondary metabolites. These phytochemicals are known for their dual functionality in nanoparticle synthesis—acting as reducing agents that facilitate the transformation of metal ions

into nanoparticles and as capping agents that enhance their stability. The CuO NPs showed a distinct peak at 292 nm, corresponding to surface plasmon resonance (SPR), which is indicative of nanoparticle formation. The presence of a broad absorption region between 400–800 nm further suggests possible nanoparticle aggregation or complex interactions in the colloidal medium. Importantly, the absence of extraneous or impurity peaks confirms the optical purity and uniformity of the synthesized nanoparticles [49].

FTIR spectral analysis substantiated the presence of functional groups essential for nanoparticle stabilization and interaction with the polymer matrix. In CuO NPs, peaks corresponding to hydroxyl, amine, carbonyl, and Cu–O vibrations confirmed the role of plant-derived biomolecules in nanoparticle formation. The starch/PVA nanoscaffold exhibited prominent absorption bands related to O–H/N–H stretching, aliphatic C–H stretching, and C=O stretching, affirming the presence of hydrophilic groups that contribute to biocompatibility. Additional bands denoting C–O–C linkages and Cu–O vibrations further corroborate the integration of CuO NPs within the scaffold. The shifts in peak positions and broadening patterns indicate strong hydrogen bonding and electrostatic interactions between the nanoparticles and the scaffold matrix, ensuring structural integrity and enhanced functional performance [50-52].

XRD analysis provided valuable insights into the crystallinity and phase purity of the CuO NPs and the nanoscaffold. The diffraction peaks of the CuO NPs matched well with the monoclinic tenorite phase, as per JCPDS card no. 05-0661, confirming the crystalline nature and phase purity of the synthesized material. Notably, the intense diffraction peaks at 22.406° and 24.107° demonstrated high crystallinity, while the broadening of peaks indicated nanoscale particle size. In contrast, the diffraction pattern of the starch/PVA nanoscaffold revealed a semi-crystalline structure with approximately 45% crystalline content. Embedded CuO was evident from shifted and reduced-intensity peaks, suggesting interactions with the polymer matrix. The observed full width at half maximum (FWHM) variations reinforced the influence of polymer blending on the scaffold's crystallinity and particle dispersion. The absence of additional peaks highlights the material's compositional purity [53, 54].

SEM images provided morphological confirmation of the successful synthesis and integration of CuO NPs within the nanoscaffold. The CuO NPs appeared as uniformly spherical particles with a narrow size distribution between 130 and 160 nm. The electrospun nanoscaffold displayed a porous fibrous architecture with fiber diameters ranging from 150 to 200 nm. Importantly, the CuO NPs were homogeneously distributed across the nanofibers without visible aggregation, suggesting effective embedding and interaction with the polymer. The smooth, bead-free fiber morphology is indicative of optimal electrospinning parameters and consistent polymer flow. This morphology is ideal for biomedical applications, as it facilitates cell adhesion, nutrient transport, and bioactivity [36, 55].

Thermal stability, a critical factor for biomedical material applications, was assessed using TGA. The scaffold displayed a three-stage degradation pattern. The initial weight loss below 150°C corresponded to moisture evaporation, while the major degradation between 220.95°C and 382.16°C reflected the breakdown of starch and PVA chains, particularly hydroxyl and glycosidic linkages. A stable residual mass beyond 382°C signified the thermal resistance of embedded CuO NPs. The thermal behavior aligns with conventional polymer degradation patterns and supports the material's feasibility for sterilization and processing under elevated temperatures [55, 56].

DLS analysis showed a monodisperse size distribution for the CuO NPs with a hydrodynamic diameter of approximately 146.1 nm, consistent with SEM results. The zeta potential was recorded at −120 mV, far surpassing the ±30 mV threshold commonly associated with high colloidal stability. This strong negative charge is a consequence of surface-bound phytochemicals, which confer electrostatic repulsion and prevent aggregation. These physicochemical properties are critical for biomedical applications where particle uniformity and dispersion are paramount [57-59].

The protein denaturation and xanthine oxidase inhibition assays demonstrated the superior anti-inflammatory activity of the starch/PVA/CuO-NPs nanoscaffold compared to the algal extract and CuO NPs alone. The concentration-dependent increase in inhibition across both assays indicated potent bioactivity. At the highest concentration tested (100 µg/mL), the nanoscaffold outperformed the CuO NPs and extract, achieving protein denaturation inhibition of 82.44% and xanthine oxidase inhibition of 80.03%, both nearing the efficacy of the standard drug. These results suggest a synergistic effect between the CuO NPs and the polymeric matrix, enhancing their anti-inflammatory potential, possibly through improved cellular uptake, sustained release, or amplified antioxidant activity [60-62].

Collectively, the characterization and biological evaluation affirm the successful synthesis and integration of CuO nanoparticles into a starch/PVA-based nanoscaffold via green synthesis [10]. The nanoscaffold exhibits favorable structural, thermal, morphological, and bioactive properties, making it a strong candidate for biomedical applications, particularly in inflammation management [63]. The synergy between plant-based synthesis, nanoscale engineering, and polymer scaffolding represents a promising strategy for developing multifunctional therapeutic platforms [64].

5. CONCLUSION

This study successfully synthesized and characterized CuO NPs using *S. wightii* algal extract, followed by their incorporation into starch/PVA nanoscaffolds for enhanced anti-inflammatory applications. UV-Visible spectroscopy confirmed nanoparticle formation via a distinct surface plasmon resonance (SPR) peak at 292 nm,

while FTIR analysis revealed functional groups responsible for stabilization and polymer interactions. XRD confirmed the monoclinic tenorite phase of CuO NPs and their successful integration into the semi-crystalline nanoscaffold structure. SEM imaging demonstrated uniform nanoparticle distribution within a porous, fibrous scaffold, ideal for biomedical applications. TGA indicated thermal stability up to 220°C, suitable for sterilization, while DLS and zeta potential measurements (−120 mV) confirmed excellent colloidal stability. Anti-inflammatory assays revealed that the starch/PVA/CuO-NPs nanoscaffolds exhibited superior inhibition of protein denaturation (82.44% at 100 µg/mL) and xanthine oxidase activity (80.03%), outperforming individual components (algal extract and CuO NPs) and closely matching the standard drug (diclofenac sodium). The enhanced efficacy is attributed to the synergistic effects of starch/PVA biocompatibility and CuO NP bioactivity. These findings highlight the nanoscaffold's potential as a therapeutic agent for inflammation-related disorders, offering a sustainable, eco-friendly alternative with optimized stability and performance. Future studies should explore *in vivo* efficacy and long-term biocompatibility for clinical translation.

Ethical Declaration: Not Applicable

Data Availability Statement: The full dataset of physiochemical characterization associated with this work is published in Mendeley Data **[Dataset]** Eco-conscious biomaterial design: Analytical insights into starch nanoscaffolds with green-engineered copper oxide nanoparticles using marine *Sargassum wightii* extract (DOI: 10.17632/vf8822rd8j.1). Disclosure: The material characterization data and figures (e.g., UV, SEM, FTIR, XRD, TGA, Zeta Potential and particle sizer) presented here were generated from a common dataset and are being reused across multiple related studies on nanomaterials. All biological analyses and conclusions are original to each manuscript.

Conflicts of Interest: The authors declare no conflicts of interest.

REFERENCES

1. Luan Y-y, Yao Y-m. The clinical significance and potential role of C-reactive protein in chronic inflammatory and neurodegenerative diseases. Frontiers in immunology. 2018;9:1302.
2. Cooke JP. Inflammation and its role in regeneration and repair: A caution for novel anti-inflammatory therapies. Circulation research. 2019;124(8):1166-8.
3. Harirforoosh S, Asghar W, Jamali F. Adverse effects of nonsteroidal antiinflammatory drugs: an update of gastrointestinal, cardiovascular and renal complications. Journal of Pharmacy & Pharmaceutical Sciences. 2013;16(5):821-47.
4. Kalelkar PP, Riddick M, García AJ. Biomaterial-based antimicrobial therapies for the treatment of bacterial infections. Nature Reviews Materials. 2022;7(1):39-54.
5. Wei J, Mu J, Tang Y, Qin D, Duan J, Wu A. Next-generation nanomaterials: advancing ocular anti-inflammatory drug therapy. Journal of nanobiotechnology. 2023;21(1):282.
6. Biris-Dorhoi E-S, Michiu D, Pop CR, Rotar AM, Tofana M, Pop OL, et al. Macroalgae—A sustainable source of chemical compounds with biological activities. Nutrients. 2020;12(10):3085.
7. Afreen A, Rasool F, Fatima M. Bioactive properties of brown seaweed, Sargassum wightii and its nutritional, therapeutic potential and health benefits: A review. Journal of Environmental Biology. 2023;44(2):146-58.
8. Fonseca-Barahona I, Shahbaz K, Baroutian S. Bioactives From Brown Algae: Antioxidant, Anti-Inflammatory, Anticancer, and Antimicrobial Potential. ChemBioEng Reviews. 2025:e70007.
9. Holghoomi R, Kharab Z, Rahdar A, Pandey S, Ferreira LFR. Harnessing the power of green synthesis of nanomaterials for anticancer applications: a review. Coordination Chemistry Reviews. 2024;513:215903.
10. Saleem MH, Ejaz U, Vithanage M, Bolan N, Siddique KH. Synthesis, characterization, and advanced sustainable applications of copper oxide nanoparticles: a review. Clean Technologies and Environmental Policy. 2024:1-26.
11. Ringu T, Das A, Ghosh S, Pramanik N. Exploring the potential of copper oxide nanoparticles (CuO NPs) for sustainable environmental bioengineering applications. Nanotechnology for Environmental Engineering. 2024;9(4):679-707.
12. Kirubakaran D, Wahid JBA, Karmegam N, Jeevika R, Sellapillai L, Rajkumar M, et al. A comprehensive review on the green synthesis of nanoparticles: advancements in biomedical and environmental applications. Biomedical Materials & Devices. 2025:1-26.
13. Khan F, Shahid A, Zhu H, Wang N, Javed MR, Ahmad N, et al. Prospects of algae-based green synthesis of nanoparticles for environmental applications. Chemosphere. 2022;293:133571.
14. Kumar Y, Singhal S, Tarafdar A, Pharande A, Ganesan M, Badgujar PC. Ultrasound assisted extraction of selected edible macroalgae: Effect on antioxidant activity and quantitative assessment of polyphenols by liquid chromatography with tandem mass spectrometry (LC-MS/MS). Algal Research. 2020;52:102114.
15. Raveesha H, Pramila L. Green Synthesis and Characterization of Copper Nanoparticles Using Urginea wightii and its Biological Activities. Indian Journal of Science and Technology. 2022;15(22):1075-83.

16. Soni V, Raizada P, Singh P, Cuong HN, Saini A, Saini RV, et al. Sustainable and green trends in using plant extracts for the synthesis of biogenic metal nanoparticles toward environmental and pharmaceutical advances: A review. Environmental Research. 2021;202:111622.
17. Ding Y, Li W, Zhang F, Liu Z, Zanjanizadeh Ezazi N, Liu D, et al. Electrospun fibrous architectures for drug delivery, tissue engineering and cancer therapy. Advanced Functional Materials. 2019;29(2):1802852.
18. Kennedy KM, Bhaw-Luximon A, Jhurry D. Cell-matrix mechanical interaction in electrospun polymeric scaffolds for tissue engineering: Implications for scaffold design and performance. Acta Biomaterialia. 2017;50:41-55.
19. Pan W, Liang Q, Gao Q. Preparation of hydroxypropyl starch/polyvinyl alcohol composite nanofibers films and improvement of hydrophobic properties. International Journal of Biological Macromolecules. 2022;223:1297-307.
20. Tabasum S, Younas M, Zaeem MA, Majeed I, Majeed M, Noreen A, et al. A review on blending of corn starch with natural and synthetic polymers, and inorganic nanoparticles with mathematical modeling. International journal of biological macromolecules. 2019;122:969-96.
21. Miculescu F, Maidaniuc A, Voicu SI, Thakur VK, Stan G, Ciocan L. Progress in hydroxyapatite–starch based sustainable biomaterials for biomedical bone substitution applications. ACS Sustainable Chemistry & Engineering. 2017;5(10):8491-512.
22. Gamage A, Punniamoorthy T, Madhujith T. Starch-based hybrid nanomaterials for environmental remediation. Starch-Evolution and Recent Advances. IntechOpen; 2021.
23. Uzair B, Syed N, Kanwal A, Samin G, Niazi MBK, Abbas S, et al. Synthesis of AgO/CuO/PVA/starch hydrogel by casting method and characterizations to safely overcome skin infections: A possible application in wound healing as a dressing. Materials Today Communications. 2024;39:109286.
24. Liu T, Xiao B, Xiang F, Tan J, Chen Z, Zhang X, et al. Ultrasmall copper-based nanoparticles for reactive oxygen species scavenging and alleviation of inflammation related diseases. Nature communications. 2020;11(1):2788.
25. Renitta RE, Narayanan R, PJ JC, Samrot AV. Antidiabetic potential of methanolic extracts of Sargassum wightii in streptozotocin induced diabetic mice. Biocatalysis and agricultural biotechnology. 2020;28:101763.
26. Akombaetwa N, Bwanga A, Makoni PA, Witika BA. Applications of electrospun drug-eluting nanofibers in wound healing: Current and future perspectives. Polymers. 2022;14(14):2931.
27. Khan MUA, Raza MA, Haider S, Shah SA, Arshed M, Abd Razak SI, et al. Medical applications of polymer/functionalized nanoparticle composite systems, renewable polymers, and polymer–metal oxide composites. Renewable Polymers and Polymer-Metal Oxide Composites. Elsevier; 2022. p. 129-64.
28. Hameed A, Hameed A, Nadeem H, Farooq T. One-pot synthesis of nanomaterials. Handbook of Greener Synthesis of Nanomaterials and Compounds. Elsevier; 2021. p. 137-76.
29. Singh YR, Selvam A, Lokhande P, Chakrabarti S. Sustainability: an emerging design criterion in nanoparticles synthesis and applications. Bioinspired and Green Synthesis of Nanostructures: A Sustainable Approach. 2023:65-113.
30. Fonseca LM, da Cruz EP, Crizel RL, Jansen-Alves C, Dias ARG, da Rosa Zavareze E. New advances of electrospun starch fibers, encapsulation, and food applications: A review. Trends in Food Science & Technology. 2024:104467.
31. Abdelrasoul GN, Farkas B, Romano I, Diaspro A, Beke S. Nanocomposite scaffold fabrication by incorporating gold nanoparticles into biodegradable polymer matrix: Synthesis, characterization, and photothermal effect. Materials Science and Engineering: C. 2015;56:305-10.
32. Osman NI, Sidik NJ, Awal A, Adam NAM, Rezali NI. In vitro xanthine oxidase and albumin denaturation inhibition assay of Barringtonia racemosa L. and total phenolic content analysis for potential anti-inflammatory use in gouty arthritis. Journal of intercultural ethnopharmacology. 2016;5(4):343.
33. Serrano JL, Figueiredo J, Almeida P, Silvestre S. From xanthine oxidase inhibition to in vivo hypouricemic effect: An integrated overview of in vitro and in vivo studies with focus on natural molecules and analogues. Evidence-Based Complementary and Alternative Medicine. 2020;2020(1):9531725.
34. Lebaudy E, Fournel S, Lavalle P, Vrana NE, Gribova V. Recent advances in antiinflammatory material design. Advanced Healthcare Materials. 2021;10(1):2001373.
35. Thuy NTT, Huy LH, Thuy Vy T, Tam NTT, Thanh BTL, My Lan NT. Green Synthesis of silver nanoparticles using Plectranthus Amboinicus leaf extract for preparation of CMC/PVA nanocomposite film. Journal of Renewable Materials. 2021;9(8):1393-411.
36. Harish V, Tewari D, Gaur M, Yadav AB, Swaroop S, Bechelany M, et al. Review on nanoparticles and nanostructured materials: Bioimaging, biosensing, drug delivery, tissue engineering, antimicrobial, and agro-food applications. Nanomaterials. 2022;12(3):457.
37. Singh AV, Chandrasekar V, Prabhu VM, Bhadra J, Laux P, Bhardwaj P, et al. Sustainable bioinspired materials for regenerative medicine: Balancing toxicology, environmental impact, and ethical considerations. Biomedical Materials. 2024;19(6):060501.
38. Asl ZR, Rezaee K, Ansari M, Zare F, Roknabadi MHA. A review of biopolymer-based hydrogels and IoT integration for enhanced diabetes diagnosis, management, and treatment. International Journal of Biological Macromolecules. 2024:135988.

39. Anbalagan G, Subramanian B, Suresh V, Sivaperumal P. Green synthesis of copper and copper oxide nanoparticles from brown algae turbinaria species' aqueous extract and its antibacterial properties. Cureus. 2024;16(4).
40. Sunarwidhi AL, Hernawan A, Frediansyah A, Widyastuti S, Martyasari NWR, Abidin AS, et al. Multivariate analysis revealed ultrasonic-assisted extraction improves anti-melanoma activity of non-flavonoid compounds in indonesian brown algae ethanol extract. Molecules. 2022;27(21):7509.
41. Rahman Khan MM, Rumon MMH, Islam M. Synthesis, Rheology, Morphology, and Mechanical Properties of Biodegradable PVA-Based Composite Films: A Review on Recent Progress. Processes. 2024;12(12).
42. Pathak V, Lad P, Thakkar AB, Thakor P, Deshpande M, Pandya S. Synthesis, characterization and applications of cubic fluorite cerium oxide nanoparticles: a comprehensive study. Results in Surfaces and Interfaces. 2023;11:100111.
43. Truzzi E, Marchetti L, Bertelli D, Benvenuti S. Attenuated total reflectance–Fourier transform infrared (ATR–FTIR) spectroscopy coupled with chemometric analysis for detection and quantification of adulteration in lavender and citronella essential oils. Phytochemical analysis. 2021;32(6):907-20.
44. Jaison JP, Balasubramanian B, Gangwar J, Pappuswamy M, Meyyazhagan A, Kamyab H, et al. Bioactive nanoparticles derived from marine brown seaweeds and their biological applications: a review. Bioprocess and Biosystems Engineering. 2024;47(10):1605-18.
45. Safari P, Rahimabadi EZ, Vaezi MR, Behnamghader A, Tahergorabi R. Development of ZnO-NPs reinforced chitosan nanofiber mats with improved antibacterial and biocompatibility properties. Sci Rep. 2025;15(1):1-17.
46. Kumar K, Srivastav S, Sharanagat VS. Ultrasound assisted extraction (UAE) of bioactive compounds from fruit and vegetable processing by-products: A review. Ultrasonics sonochemistry. 2021;70:105325.
47. Chaiya P, Senarat S, Phaechamud T, Narakornwit W. In vitro anti-inflammatory activity using thermally inhibiting protein denaturation of egg albumin and antimicrobial activities of some organic solvents. Materials Today: Proceedings. 2022;65:2290-5.
48. Trinh PTN, Truc NC, Danh TT, Trang NTT, Le Hang DT, Vi LNT, et al. A study on the antioxidant, anti-inflammatory, and xanthine oxidase inhibitory activity of the Artemisia vulgaris L. extract and its fractions. Journal of Ethnopharmacology. 2024;334:118519.
49. Hasan EA, El-Hashash MA, Zahran MK, El-Rafie HM. Comparative study of chemical composition, antioxidant and anticancer activities of both Turbinaria decurrens Bory methanol extract and its biosynthesized gold nanoparticles. Journal of Drug Delivery Science and Technology. 2022;67:103005.
50. Maji P, Pal D. Phytosynthesized copper oxide nanoparticles and their application in Pb2+ detection from surface water. Applied Physics A. 2024;130(9):637.
51. Nandiyanto ABD, Ragadhita R, Fiandini M. Interpretation of Fourier transform infrared spectra (FTIR): A practical approach in the polymer/plastic thermal decomposition. Indonesian Journal of Science and Technology. 2023;8(1):113-26.
52. Pasieczna-Patkowska S, Cichy M, Flieger J. Application of Fourier Transform Infrared (FTIR) Spectroscopy in Characterization of Green Synthesized Nanoparticles. Molecules. 2025;30(3):684.
53. Ali K, Sajid M, Bakar SA, Younus A, Ali H, Rashid MZ. Synthesis of copper oxide (CuO) via coprecipitation method: Tailoring structural and optical properties of CuO nanoparticles for optoelectronic device applications. Hybrid Advances. 2024;6:100250.
54. Paul CA, Kumar ER, Suryakanth J, Abd El-Rehim A. Analysis and characterization of structural, morphological, thermal properties and colloidal stability of CuO nanoparticles for various natural fuels. Ceram Int. 2023;49(19):31193-209.
55. Le TDH, Tuan HNA, Nguyen VT, Le AT. Hydroxyapatite− loaded starch/polyvinyl alcohol scaffold for bone regeneration application: preparation and characterization. Journal of Sol-Gel Science and Technology. 2023;107(2):441-51.
56. Ramezani M, Ripin ZM. An overview of enhancing the performance of medical implants with nanocomposites. Journal of Composites Science. 2023;7(5):199.
57. Alhalili Z. Green synthesis of copper oxide nanoparticles CuO NPs from Eucalyptus Globoulus leaf extract: Adsorption and design of experiments. Arabian Journal of Chemistry. 2022;15(5):103739.
58. Pochapski DJ, Carvalho dos Santos C, Leite GW, Pulcinelli SH, Santilli CV. Zeta potential and colloidal stability predictions for inorganic nanoparticle dispersions: Effects of experimental conditions and electrokinetic models on the interpretation of results. Langmuir. 2021;37(45):13379-89.
59. Yu C, Dou X, Meng L, Feng X, Gao C, Chen F, et al. Structure, rheological properties, and biocompatibility of Laponite® cross-linked starch/polyvinyl alcohol hydrogels. International Journal of Biological Macromolecules. 2023;253:127618.
60. Al-Dulaimy WYM, Hussein AA, Mahdi MA, Kadhom M. In Vitro Inhibition of Xanthine Oxidase Purified from Arthritis Serum Patients by Nanocurcumin and Artemisinin Active Compounds. Molecules. 2023;28(13):5124.
61. Mendez-Encinas MA, Valencia D, Ortega-García J, Carvajal-Millan E, Díaz-Ríos JC, Mendez-Pfeiffer P, et al. Anti-inflammatory potential of seasonal sonoran propolis extracts and some of their main constituents. Molecules. 2023;28(11):4496.

62. Kola P, Metowogo K, Manjula S, Katawa G, Elkhenany H, Mruthunjaya K, et al. Ethnopharmacological evaluation of antioxidant, anti-angiogenic, and anti-inflammatory activity of some traditional medicinal plants used for treatment of cancer in Togo/Africa. Journal of Ethnopharmacology. 2022;283:114673.
63. Du Z, Cao G, Li K, Zhang R, Li X. Nanocomposites for the delivery of bioactive molecules in tissue repair: vital structural features, application mechanisms, updated progress and future perspectives. Journal of Materials Chemistry B. 2020;8(45):10271-89.
64. Iravani S, Varma RS. Plants and plant-based polymers as scaffolds for tissue engineering. Green Chemistry. 2019;21(18):4839-67.

Figures

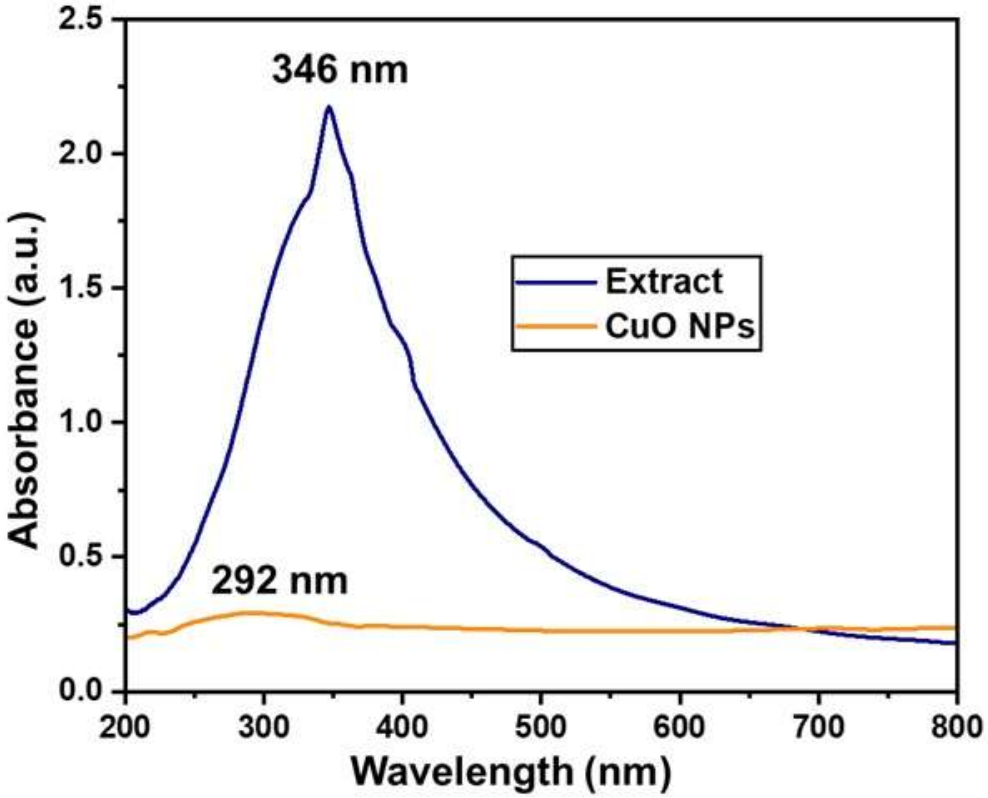

Fig. 1. UV–Visible spectral profiles of algal extract and CuO nanoparticles.

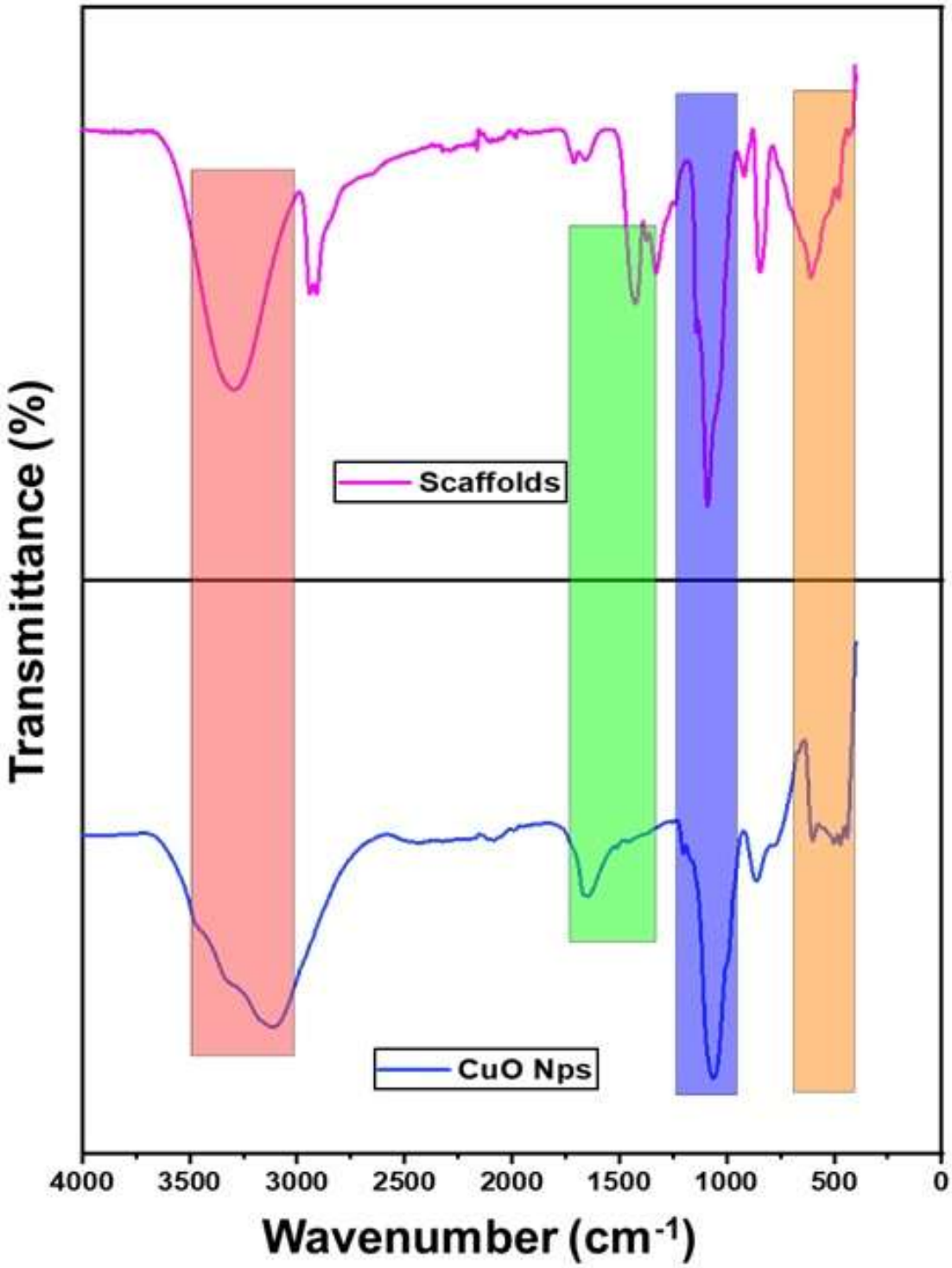

Fig. 2. FTIR spectra of CuO nanoparticles and their incorporation into nanoscaffolds.

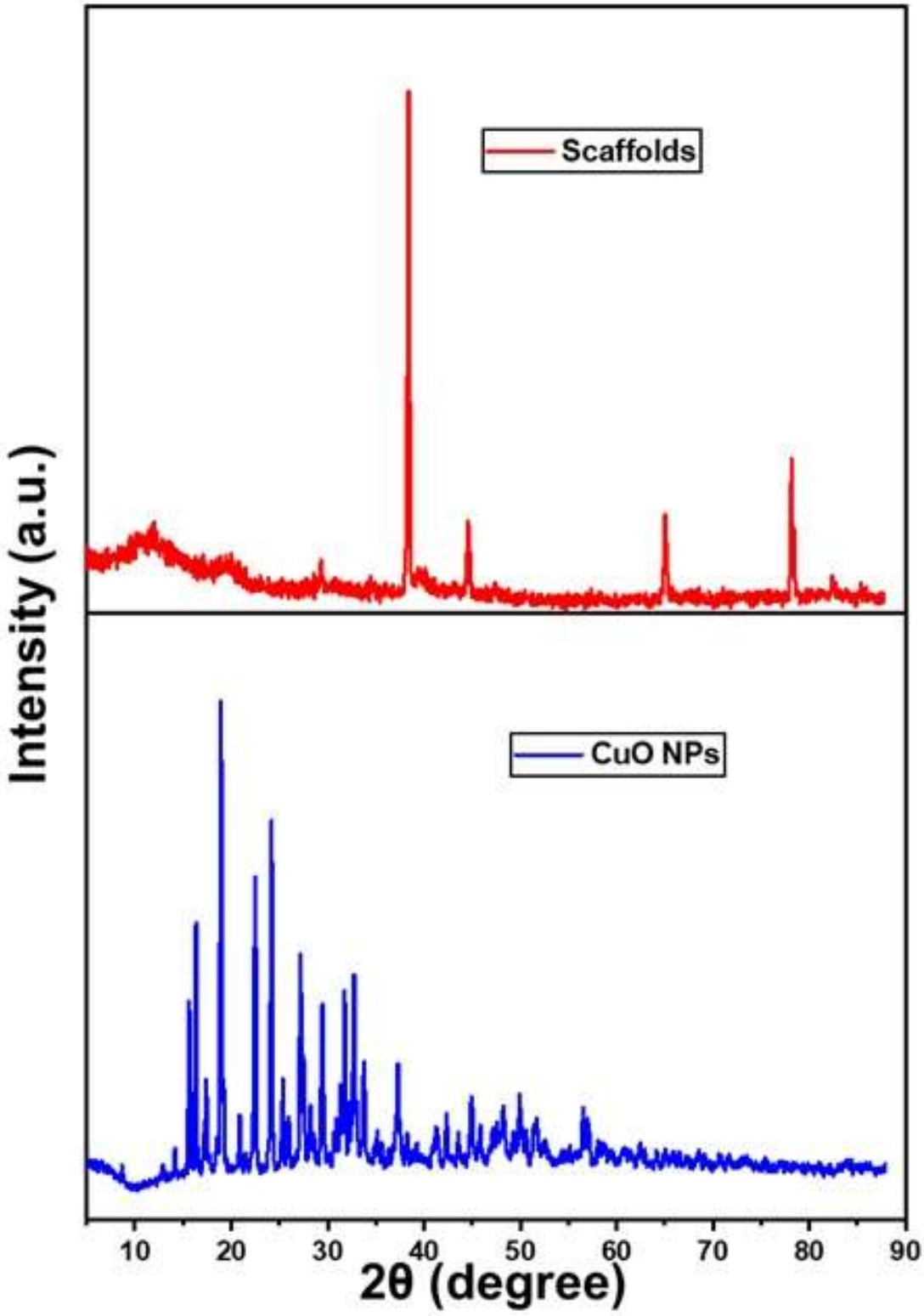

Fig. 3. XRD patterns of synthesized CuO nanoparticles and CuO-loaded scaffolds.

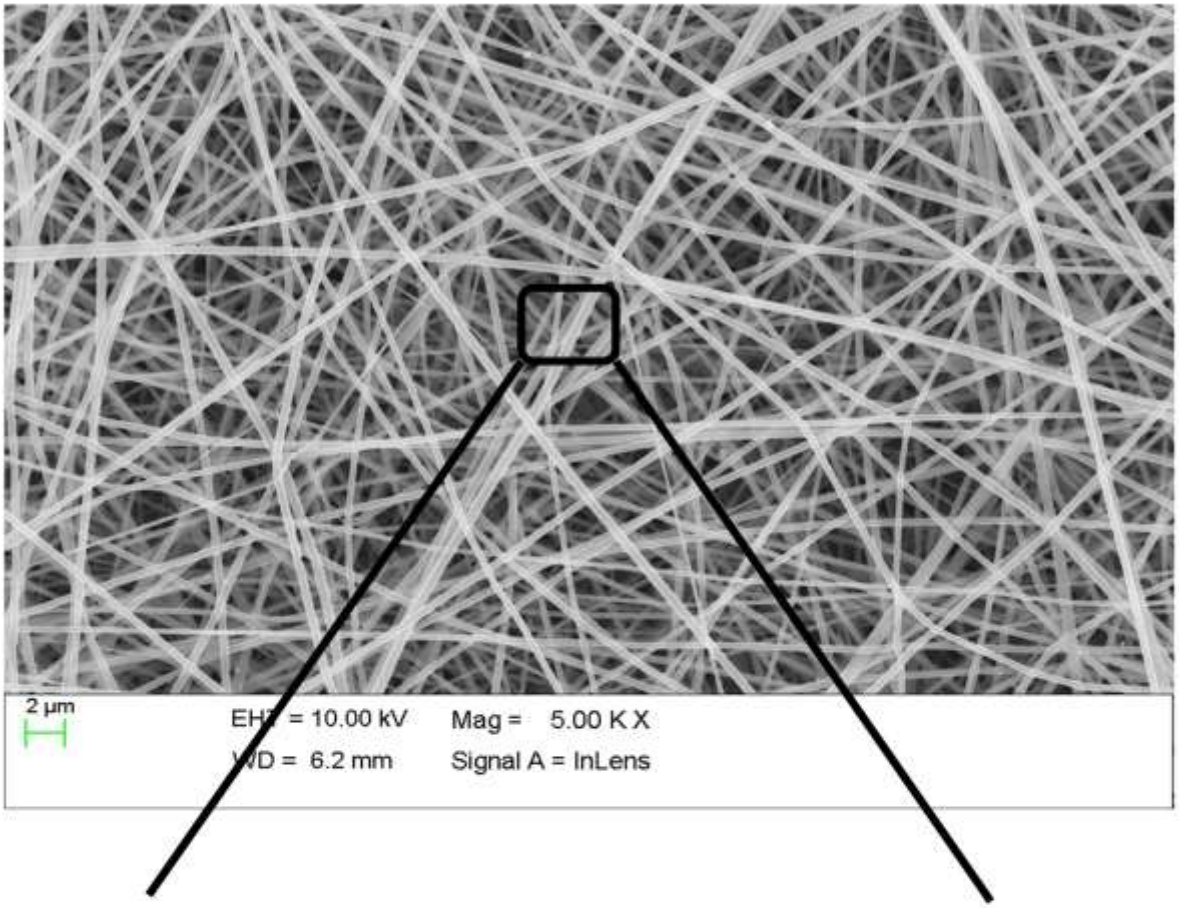

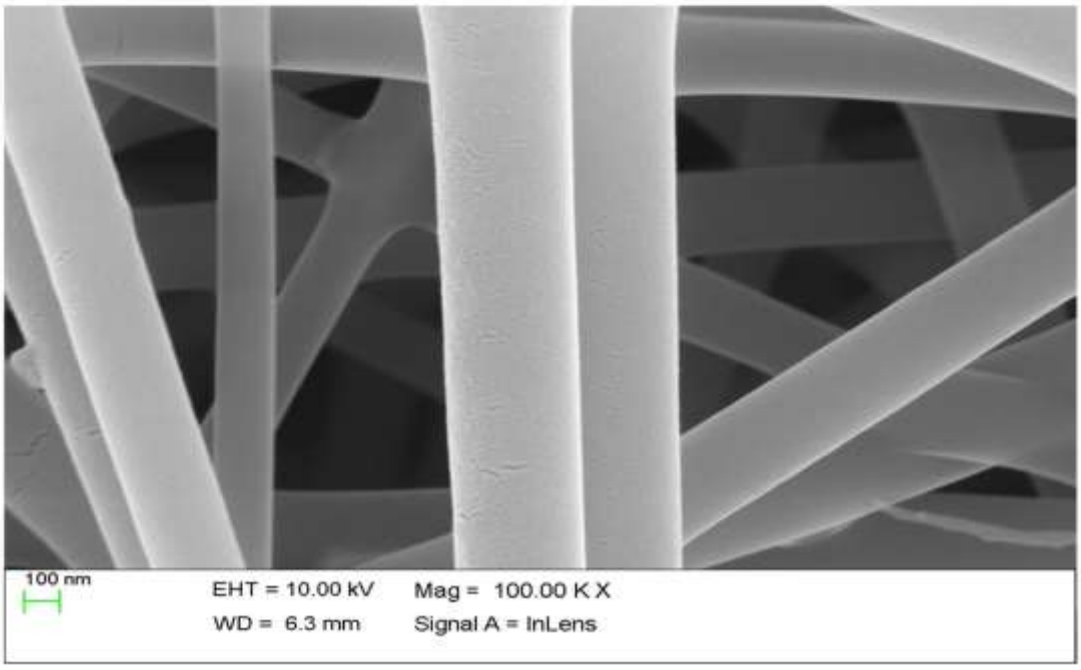

Fig. 4. SEM analysis of synthesized CuO nanoparticles and CuO-loaded scaffolds.

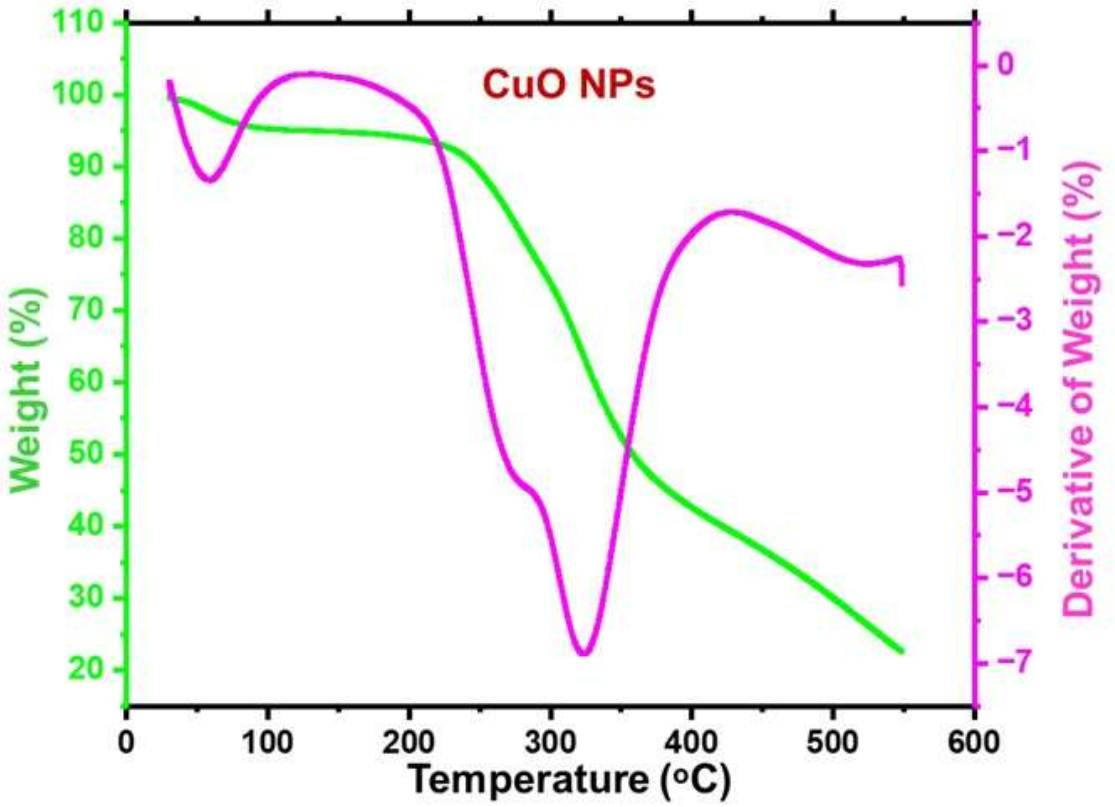

Fig. 5. Thermal degradation behavior of CuO-incorporated nanoscaffolds.

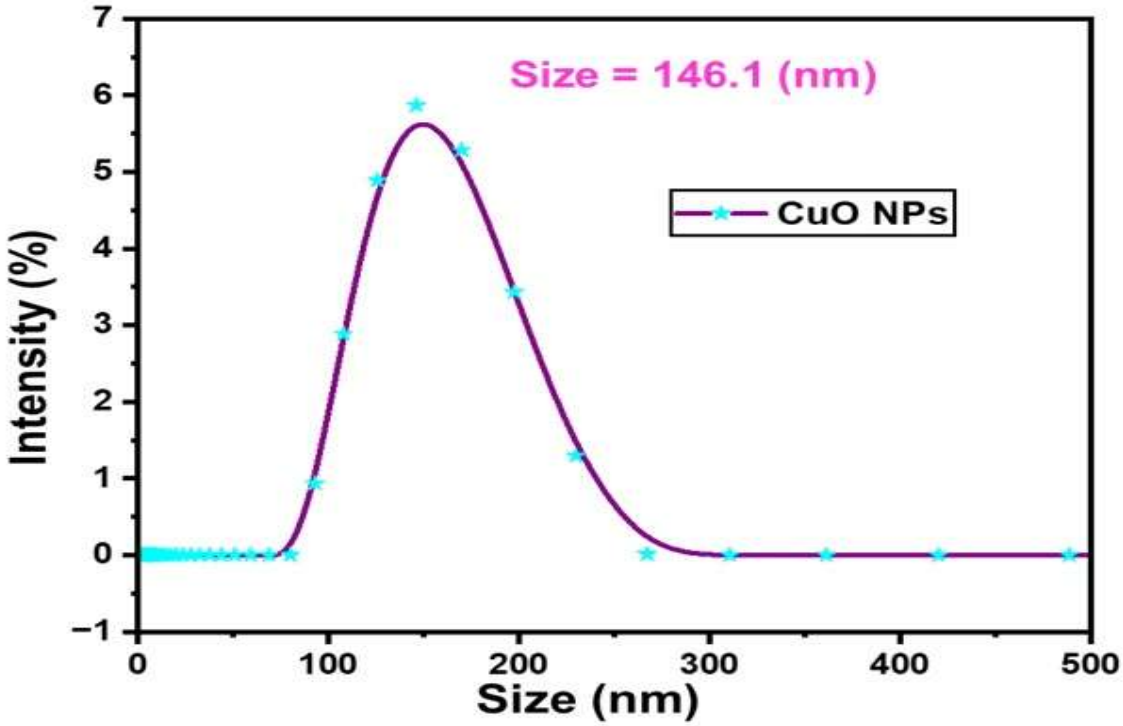

Fig.6. DLS particles size analysis of CuO NPs

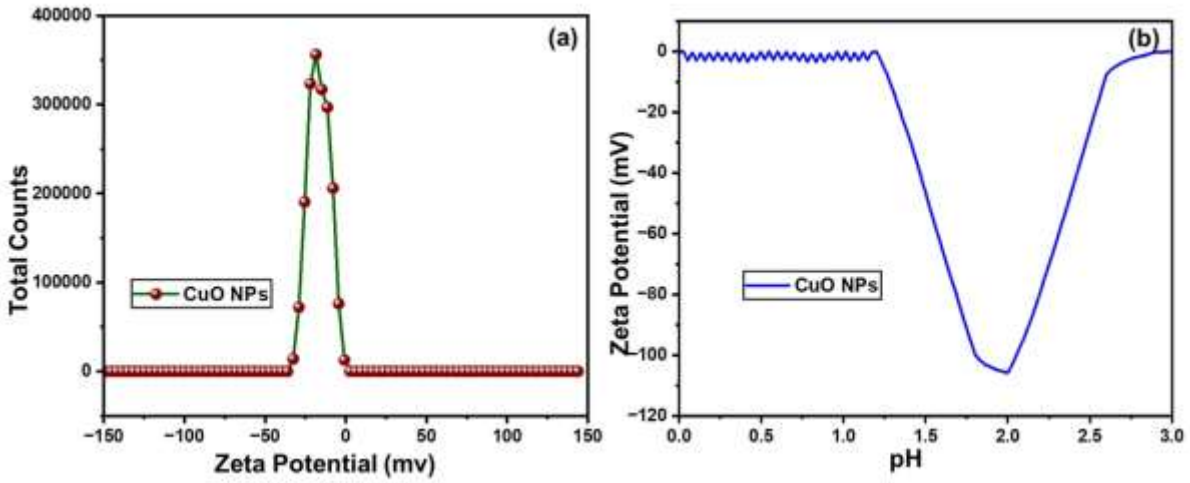

Fig.7. Zeta-potential analysis of CuO NPs

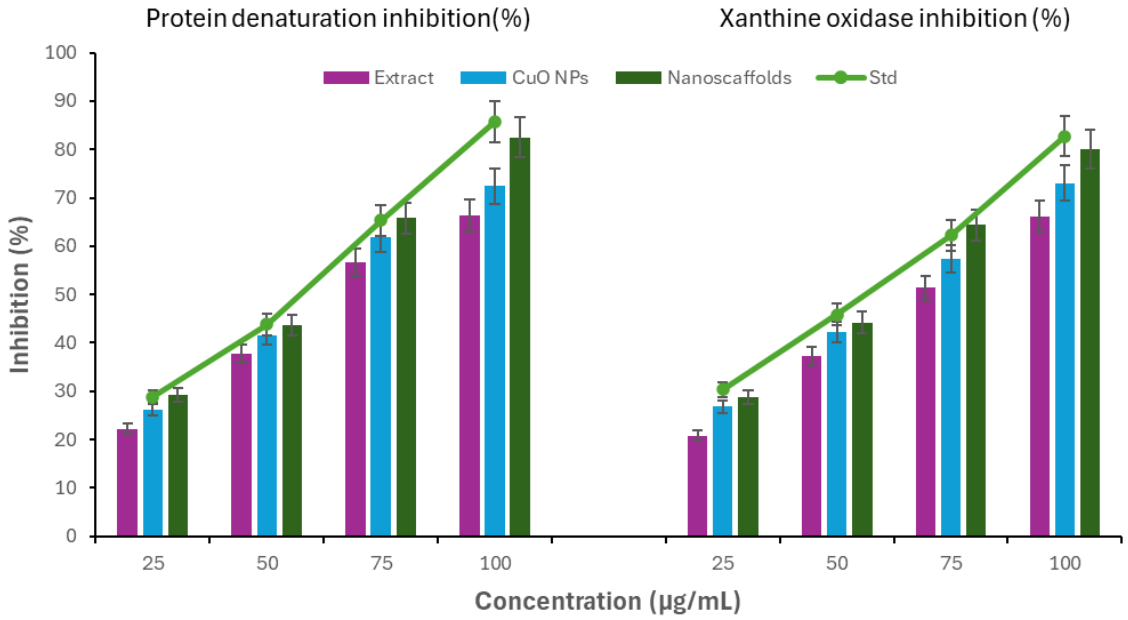

Fig.8. Anti-inflammatory activity analysis of algal extract, CuNPs and starch/PVA/CuONPs nanoscaffolds